Combined mixing and dynamical origins of T_g alterations near polymer-polymer interfaces

Asieh Ghanekarade[a] and David S. Simmons[a*]

[a]Department of Chemical, Biological, and Materials Engineering, University of South Florida, Tampa, Florida, 33544.

[*]Corresponding author e-mail: dssimmons@usf.edu

Abstract: The extent to which altered glass formation behavior in block copolymers and layered polymers results simply from local compositional mixing vs from longer-ranged dynamical correlations has long been unresolved. This question has become particularly acute over the last several decades, as a large literature has emerged demonstrating the presence of long-ranged dynamical gradients at polymer interfaces (such as free surfaces and substrates) that lack mixing effects. Here, we perform molecular dynamics simulations of glass formation at model polymer-polymer interfaces to understand the relative roles of these mechanisms in altering dynamics and glass formation at interfaces in medium molecular weight polymers. Results indicate a crossover in mechanism from the high-χ regime, where dynamical T_g alterations near the interface are driven purely by dynamical gradient effects, to the low χ regime, where both local mixing and dynamical correlations play a role. Gradients observed in simulation are asymmetric, with a larger domain size required to recover bulk-like T_g on the high-T_g side than the low-T_g side of the interface. T_g gradient ranges are observed to grow with decreasing χ (and to generally exceed the range of composition gradients), but the overall practical range for recovery of bulk-like T_g remains of order 10 nm over approximately two orders of magnitude variation in χ. These results provide new insight into the design of block copolymers and other nanostructured polymers with targeted local dynamics relevant to applications such as battery materials and separations. Our results also emphasize and clarify a significant mystery surrounding an apparent dichotomy between a large number of simulation and experimental results, including ours, pointing towards T_g gradient ranges on the order of 10 nm, and a second set of studies reporting on longer ranges up to hundreds of nm.

Introduction

Dynamics near interfaces in glass-forming liquids commonly exhibit significant alterations compared to bulk, with shifts in the glass transition temperature T_g reported to reach 50 K or more[1–8]. These alterations impact a wide range of polymeric systems[9], including thin films[6,10–16], semicrystalline polymers[17–21], polymer nanocomposites[22–24], ionomers[25–30] and block and layered[31–38] polymers. A substantial portion of the research on these effects has focused on polymers in contact with free surfaces or hard interfaces, such as rigid substrates or particles. There, these shifts are primarily driven by large gradients that are almost purely dynamical in nature, being far longer ranged than any associated interfacial thermodynamic or structural gradient[1]. A smaller body of work has probed related effects in the vicinity of polymer-polymer interfaces[31–49]. Here, interfacial intermixing can yield broader thermodynamic gradients. The

manner in which these broader thermodynamic gradients interact with polymers' tendency towards long-ranged dynamical gradients remains poorly understood – an open question that is relevant to a wide range of multi-phase polymeric systems.

An understanding of the relative roles of thermodynamic intermixing at the interface vs dynamical gradient effects would be relevant to the design and understanding of block copolymers and layered polymers, including their glass transition temperature and mechanical response. Indeed, a number of studies have probed altered dynamics in the interfacially-rich environment provided by block copolymers and have come to a range of disparate conclusions. For example, Robertson et al. probed the T_g of polystyrene (PS) domains in styrene-co-butadiene soft block copolymers with domain sizes ranging from 20 nm to 70 nm, and they argued that T_g shifts relative to the homopolymer were controlled by the miscibility of the two blocks and therefore were thermodynamically controlled[43]. However, more local data on a similar system paints a more complex picture. In particular, based on measurements of *local* glass transition temperature gradients at interfaces in PMMA/PBMA copolymers, Christie et al. determined that T_g gradients are not fully accounted for by composition gradients at these interfaces, even considering self-concentration effects[32,50]. Simulations of diblock copolymers[31] and gradient copolymers[40] by Slimani et al. suggest the presence of much broader dynamical gradients in gradient than block copolymers due to the presence of longer-ranged compositional gradients. However, simulations of block copolymers in cylindrical and spherical morphologies suggested that the Flory-Fox and Lodge-McLeish T_g mixing rules do not correctly describe the dynamical gradients in these systems, in qualitative accord with the findings of Christie et al.[50,51]

A complementary body of work has also probed T_g shifts at interfaces in layered polymers. There are potentially several differences here relative to block copolymers. First, here there are no intrachain covalent junctions between the two chemical moieties. Second, in this case domain sizes can potentially far exceed those in block copolymers. Early work by Torkelson and coworkers suggested that layered polymers are essentially equivalent to block copolymers in terms of T_g effects[33]. More recent work by Roth and coworkers reported on spatially resolved T_g gradients at an interface between two layered polymers[34,41,52]. The overall range of these gradients was reported to be[34,41,52] more than an order of magnitude larger than those observed by Christie et al.[51] in the block copolymer system. Notably, the composition gradients in Baglay et al.'s nanolayered polymer systems are still only of order 5 nm – considerably longer-ranged than at a sharp interface but still dramatically shorter-ranged than the 100's of nm range T_g gradients they report. These and other results from the Roth group employing this methodology point to extraordinarily long-ranged T_g gradients at some polymer-polymer interfaces that far outstrip the range of any posited composition gradient in the system[34,36,41].

At the same time that these experiments indicate that gradients at polymer-polymer interfaces retain a uniquely dynamical character, they also emphasize complexities suggesting sensitivity of the T_g gradient to the presence of a broad thermodynamic interface. Both the works of Christie et al.[32,50] and those of Roth and coworkers[34,41,52] reported a characteristic asymmetry of the T_g gradient, with stronger gradients observed on the high T_g side of the interface as compared to the low-T_g side. In contrast, a prior simulation study of polymer-polymer interfaces reported fairly

symmetric dynamical gradients[53], raising questions as to whether those simulations simply coincidentally probed a different regime of behavior or if some other factor was at work. In the asymmetric results observed in experiment, Christie et al. reported on evidence for a mixed dynamic/thermodynamic effect, wherein composition gradients played an important role in defining the T_g gradient on the low-T_g side of the interface.

Perhaps most strikingly and as suggested above, the T_g gradients reported by Baglay et al. were of range far greater than that typically associated with T_g gradients at rigid substrates or free surfaces, potentially suggesting that the broad nature of the polymer-polymer interface somehow led to much longer-ranged T_g gradients. Indeed, their works suggested that the massive ranges they observe only develop upon sufficient annealing of the interface to allow a full composition gradient to develop[41]. Their work also suggested that higher-χ interfaces possessing sharper composition gradients tend to exhibit reduced (but still immensely large compared to the composition gradient range) gradient ranges relative to interfaces with broader composition gradients[52].

On the one hand, it is well-established that dynamical gradients at thermodynamically sharp (i.e. hard or free surface) interfaces are far longer ranged than thermodynamic gradients[1]. One would logically expect this scenario to hold in the extremely high χ limit of very sharp polymer-polymer interfaces. On the other hand, the findings above begin to extend this understanding to thermodynamically broader polymer-polymer interfaces: (1) the breadth of thermodynamic gradients plays a role (if currently poorly understood) in setting the strength and range of dynamical gradients; however, (2) dynamical gradients are not *locally* controlled by thermodynamic gradients in any simple way. This latter finding is consistent with a broader literature indicating that dynamical gradients at interfaces in glass-forming liquids are not locally driven by thermodynamic or structural gradients[1]. Given this complexity, the precise relationship between compositional and dynamical gradients at polymer-polymer interfaces remains a significant open question in the field.

These findings collectively raise a number of questions. What is the nature of the crossover between the T_g behavior observed in the high χ (sharp interface) and low χ (broad interface) regimes? Could a crossover of this kind be at play in the differing results prior simulations vs experiments have reported with respect to the asymmetry of the interfacial gradient? What is the interplay between thermodynamic and dynamical gradients in the low χ regime and how does this determine the overall T_g shift? Could the presence of a broad thermodynamic interface, combined with a large domain size, somehow lead to an orders of magnitude longer ranged dynamical gradient?

In this work, we employ simulations of layered bead-spring polymers (explicitly modeling two layers, with periodic boundary conditions), over a large χ range, to gain insight into the answers to these questions. We employ large domain sizes (of order 34 bead diameters σ_{LJ} for high χ and 45 σ_{LJ} for low χ) to ensure that the range of dynamical gradients has space to fully develop, which has been shown to be important experimentally[54] in observing the full gradient effect. Simulations focus on 96-bead chains, which is somewhat above the reported entanglement

weight for this polymer; such that these chains are fairly long on the scale of typical bead-spring simulations probing glass formation behavior under nanoconfinement. However, they are still considerably shorter than many experiments employing polymers with molecular weights in the range of several hundred kg/mol. We emphasize that the choice of molecular weight can play an important role in mediating between the value of χ and the breadth of the interfacial composition gradient, at least in the low molecular weight range. In general, because we are at lower molecular weights than many experiments, we expect that our simulations to involve modestly broader interfacial composition gradients than those experiments, *when compared at equal χ*. However, based on field theoretic calculations by Broseta et al., our chains are likely reasonably close to the high molecular weight plateau regime in which the interface becomes molecular weight insensitive, and deviations from this limit in our simulations are expected to be fairly small[55]. We discuss the implications of these issues in comparing our findings to experiment further below.

Our results indicate that gradients in glass transition temperature and dynamics are always longer-ranged than composition gradients, over a wide range of χ. However, we find that while these gradients are essentially purely dynamical in the high-χ limit, they transition to a distinct mixed thermodynamic/dynamic character with decreasing χ / increasing gradient range. Moreover, we find longer-ranged gradients on the high-T_g side of the interface than the low-T_g side, consistent with experiment, while we find the asymmetry in the *magnitude* of the gradient on each side of the interface is χ-dependent. Collectively, these findings point to the presence of two regimes of T_g gradient behavior at polymer-polymer interfaces – a low χ regime and a high-χ regime, with the physics driving long-ranged dynamical gradients playing an important role in both. Our results do not reveal any evidence for extraordinarily long-ranged T_g gradients on the order of 100 nm in the equilibrium dynamics of these polymers, and we discuss possible scenarios for why these gradients may appear in some experiments but not in the systems probed here or in multiple other related simulation and experimental studies.

Methodology

We simulate layered polymer films comprised of 96-bead model polymer chains, in which the two layers possess innately differing T_g values. Simulations employ a modified variant of the attractive Kremer-Grest bead spring model[40], possessing shortened bonds to better suppress crystallization[56]. Within this model, non-bonded beads of types *i* and *j* interact via the 12-6 binary Lennard-Jones (LJ) potential,

$$E_{ij} = 4\varepsilon_{ij}\left[\sigma^{12}r^{-12} - \sigma^{6}r^{-6}\right], \quad (1)$$

where the interaction is truncated at r_{cut} = 2.5 σ_{LJ} (where σ_{LJ} is the LJ unit of length and is of order 1 nm in real units) and where in all cases σ = 1σ_{LJ}. Bonded beads interact via a combination of the Finitely Extensible Nonlinear Elastic (FENE) and 12-6 LJ potentials,

$$E_{b,i} = -\frac{1}{2}K_i R_0^{\,2}\ln\left[1-\left(\frac{r}{R_0}\right)^2\right] + 4\varepsilon_{b,i}\left[\sigma_b^{\,12}r^{-12} - \sigma_b^{\,6}r^{-6}\right], \quad (2)$$

where the second term is truncated at its minimum of $2^{1/6}$ σ_b and where we employ range parameters of R_0 = 1.3 and σ_{bond} = 0.8 – values that are reduced from their typical values in order to confer enhanced crystallization resistance[56]. This general class of bead-spring model has been widely employed to successfully probe nanoconfinement and interface effects on the glass transition[6,16,17,35,57–72].

We implement a T_g differential within the layered polymer by employing differential energy parameters for both bonded and nonbonded interactions. For the first polymer, we employ ε_{11} = 1.0, K_1 = 30, and $\varepsilon_{b,1}$ = 1.0. For the second polymer, we employ energy parameters enhanced by a factor of 1.3; i.e. ε_{22} = 1.3, K_1 = 39, and $\varepsilon_{b,1}$ = 1.3. As shown in prior works[35,73], this produces a situation in which the bulk T_g values of the two polymers differ by 30%; i.e. $T_{g2}^{Bulk} = 1.3T_{g1}^{Bulk}$.

We then tune the value of χ and thus the breadth of the thermodynamic interface between this pair of polymers by tuning the cross-interaction energy parameter ε_{12} over a wide range of values: 0.25, 0.6, 0.75, 0.9, 1.05, 1.12, 1.13, 1.14, 1.142, 1.146, and 1.148. In a simple Flory-Huggins type picture, one expects the χ parameter to be proportional to the exchange parameter Δε between the two species:

$$\chi_{FH} = \frac{\zeta \Delta\varepsilon}{2k_B T} \ , \qquad (3)$$

where

$$\Delta\varepsilon \equiv \left(\varepsilon_{11} + \varepsilon_{22} - 2\varepsilon_{12}\right), \qquad (4)$$

and where k_B is Boltzmann's constant, T is temperature, and ζ is some effective neighbor count. Employing ζ = 10 as a reasonable close-order estimate of typical neighbor counts in bead-based models and k_BT = 0.5 as a reasonable temperature value reflecting a point in the glass formation range for this class of model, this suggests indicates that our simulations span a χ range spanning about two orders of magnitude. Below in the results section we compare these expectations to χ values inferred more directly from the interfacial composition gradient rather than estimated from theory.

Simulations employed the Large-scale Atomic/Molecular Massively Parallel Simulator (LAMMPS) molecular dynamics simulation package[74], with all simulations using Verlet integration and a 0.005 τ_{LJ} time step (where τ_{LJ} is the LJ unit of time and corresponds approximately to a picosecond). All simulations employ the Nose-Hoover Thermostat/Barostat pair as implemented in LAMMPS, with damping parameters of 2 τ_{LJ}. Pressures P are set to 0.

For layered simulations, numbers of chains are selected to produce polymer layers of sufficient thickness that the dynamics are nearly bulk-like in the mid-film. For simulations with $\varepsilon_{12} \leq 1.14$, 602 chains of each type are simulated with lateral dimensions of 34 σ_{LJ} x 34 σ_{LJ}, which yields lamellar layer thicknesses of about 34 σ_{LJ} at T=0.5. For simulations with $\varepsilon_{12} > 1.14$, the number of chains of each species is increased to 752, which yields layer thicknesses in the range of 45 σ_{LJ} at T=0.5, in order to accommodate the additional space needed for the broader thermodynamic interfaces in these systems. Simulations are performed with periodic boundary conditions in all

directions, such that systems effectively consist of a stack of alternating layers with two modeled explicitly.

Initial configurations were created in a layered configuration by PACKMOL[75]. These configurations were then equilibrated at a high temperature T=1.4 in LJ units for 1.5 x 10^8 τ_{LJ} for high χ systems and for 10^9 τ_{LJ} for low χ systems. The longer times allowed at lower χ ensure full interdiffusion of the longer-ranged thermodynamic interfaces present in these systems. Corresponding bulk simulations are performed with 602 chains of each type. As an additional verification that these times were sufficient for good interface formation, we simulated the mixing of two initially separate layers of polymer (at the same molecular weight as our primary simulations), but with a cross-interaction parameter favoring full miscibility, as described below. The times above were more than sufficient to enable full mixing of that control system.

Translational dynamics are quantified via the self-intermediate scattering function, computed at a wavenumber of q = 7.07, corresponding to approximately the first peak in the segmental structure factor. Relaxation times were computed by fitting the long-time response of this relaxation function to the Kohlraush-Williams-Watts (KWW) stretched exponential function for data smoothing and interpolation, and then defining the relaxation time τ as the time at which this function relaxes to a value of 0.2. This set of conventions for translational relaxation time determination is widely employed in the simulation literature[64,67,76,77].

Relaxation time analysis is performed both at a whole layer level and locally, by first binning particles into bins of thickness 0.875 as a function of distance from the interface (defined as the plane at which the mole fraction of both segment types is 0.5) and then performing the above analysis on particles in these local bins. Glass temperatures defined on a computational timescale are calculated by fitting the temperature dependence of the above relaxation time to the Vogel-Fulcher-Tammann (VFT)[78,79] equation and extracting the temperature at which the relaxation time is 10^4 τ_{LJ}. We show in supplementary figures 1 and 2 that the VFT form provides excellent fits to local relaxation data in these simulated systems. This convention of defining a computational T_g at a timescale around the upper limit of equilibrium simulations times is commonly employed in the simulation literature[67,80–82]. By this set of conventions, the bulk T_g of the low-T_g and high-T_g polymers are 0.417 and 0.549, respectively, in Lennard Jones temperature units.

Results

Composition gradients and χ parameter

We begin by quantifying the dependence of χ on the exchange parameter Δε (as controlled directly by the cross-interaction parameter ε_{12}), since χ is the key variable in tuning the interface breadth at fixed molecular weight. A more direct estimation of the χ parameter than can be obtained via the Flory-Huggins approach from equations (3) and (4) can be extracted by comparing interfacial composition gradient to field theoretical calculations. On the basis of such calculations, Semenov suggested that the gradient of component A across the interface can be described by the following functional form[83]:

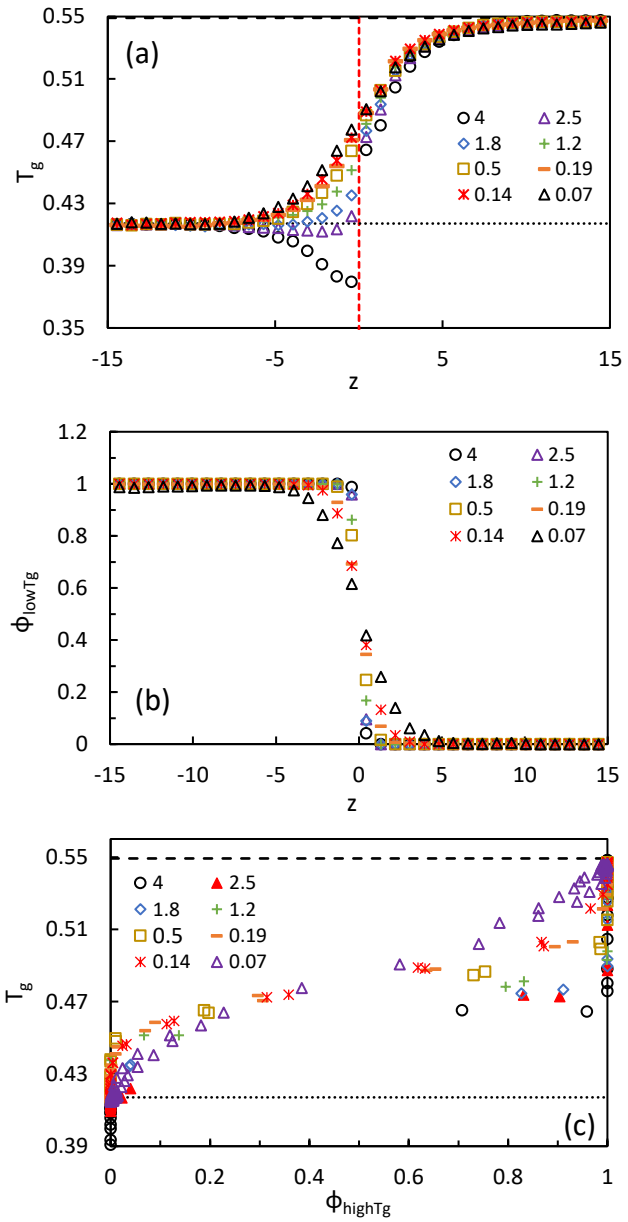

Figure 1. (a) T_g of layered polymers as a function of distance z from an interface. χ values for each dataset, computed via equation (4), are shown in the legend. The z>0 domain corresponds to the predominantly high-T_g polymer domain, and the z<0 domain to the predominantly low-T_g polymer domain, (b) Local composition fraction of low-T_g polymer, for the same systems shown in part a, as a function of distance z from the interface (c) Local T_g plotted vs local fraction low-T_g polymer. In parts (a) and (c), the dashed line and dotted line represent the bulk-state T_g's of the high-and low-T_g polymers, respectively.

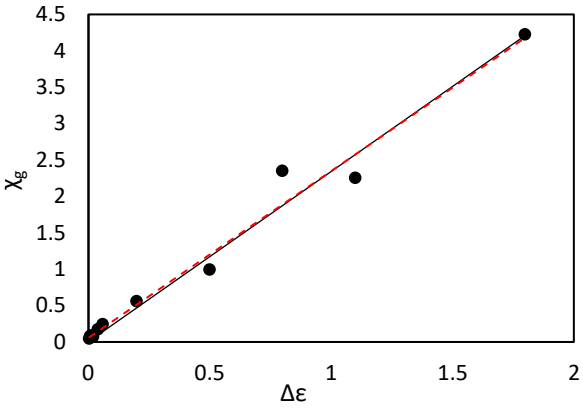

Figure 2. χ parameters computed from fits of composition gradient data to equations (5) and (6), plotted vs the exchange parameter defined by equation (4). Solid line is a fit to a proportionality, $\chi_g = (2.24)\Delta\varepsilon$ Dashed red line is a fit to a linear form, $\chi_g = (2.20 \pm 0.225)\Delta\varepsilon + (0.564 \pm 0.150)$.

$$\phi_A(z) = \frac{1}{2}\left[1 + \tanh\frac{2z}{\Delta}\right], \qquad (5)$$

where Δ is a measure of the breadth of the interface and is directly controlled by χ. Earlier work by Broseta et al. derived from field theoretic calculations the relationship between Δ and χ in the case of a finite molecular weight chain[55]. In the case of two immiscible, monodisperse polymers comprised of chains of equal degree of polymerization n, their equation reduces to

$$\frac{\Delta(n)}{a} = 2\chi^{-1/2}\left[1 - \frac{4\ln 2}{\chi n}\right]^{-1/2} . \qquad (6)$$

Here, *n* is the number of segments in the chain, and *a* is the statistical segment length. Based on gyration radius data for the bulk simulated bead spring polymer, we calculate *a* = 1.22, with prior work indicating that the Kuhn segment (and thus statistical segment length) is fairly temperature-insensitive for this polymer. Accordingly, we compute composition gradients across the polymer-polymer interface at a temperature of approximately 0.5 in reduced Lennard Jones units (see Figure 1a), and we fit them to equation (5) to obtain a composition gradient

breadth Δ for each system. We then employ equation (6) to infer a value of χ on the basis of this gradient breadth data.

As shown by Figure 2, χ_g (the value of χ as inferred from the gradient) is nearly proportional to Δε within uncertainty, as expected from equation (3). A slightly improved fit can be obtained to a linear form containing a constant term to allow for the possibility of a deviation from the Flory prediction that χ = 0 when Δε = 0. This fit suggests modest deviations from the Flory-Huggins expectation for the χ = 0 condition (which expects this to hold when ε_{12} = 1.15), finding that χ = 0 when ε_{12} = 1.16. However the uncertainty on this parameter encompasses the Flory-Huggins expectation and so it does not provide strong evidence of an alternative scenario on its own.

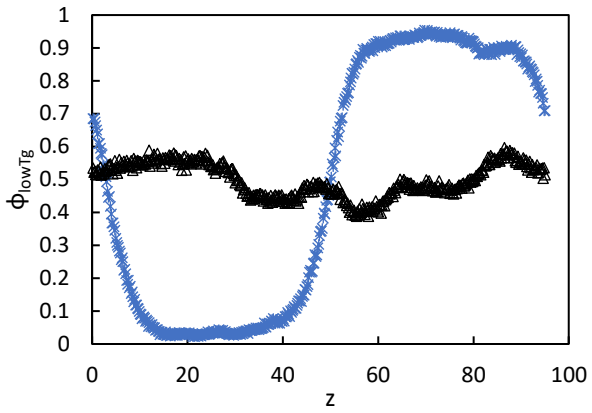

Figure 3. Composition profiles for system with ε_{12} = 1.15 (blue x's) and 1.155 (black triangles), at a temperature of 1.4 in reduced LJ units.

With this in mind, we performed simulations at the anticipated Flory-Huggins χ = 0 condition (ε_{12} = 1.15, Δε = 0) and slightly beyond this condition (ε_{12} = 1.155) to assess whether an upward deviation from the Flory-Huggins scenario is genuinely present in our χ model. As shown by Figure 3, the system does not fully mix at ε_{12} = 1.15 but does fully mix at ε_{12} = 1.155. This suggests that the zero χ condition does require at least a slightly-stronger cross-interaction than anticipated by the Flory Huggins model. Moreover, because these chains are of finite molecular weight, mixing is expected at slightly positive χ. We thus conclude that the fit value of 1.16 obtained based on the fits to gradient forms above is reasonable. Throughout the remainder of this paper, we therefore report χ values for each system obtained via the best fit linear relation observed above, i.e.

$$\chi = 2.20\Delta\varepsilon + 0.564 \,. \qquad (7)$$

Relationship between T_g and composition gradients

We continue by quantifying the interfacial T_g gradients present in these systems and probing the extent to which local variation in T_g can be understood based upon local variation in composition ϕ (defined as the fraction of beads of a given type at a distance z from the interface) within a local-mixing perspective. T_g gradients for a representative subset of systems are depicted in Figure 1b. As can be seen here, gradients on the low-T_g side of the interface exhibit a profound dependence on χ, with a transition from local T_g suppression in the ultra-high χ limit (previously show to be associated with a local density suppression at the interface in this limit[35]) to T_g enhancement observed with increasing χ. The χ-dependence of T_g on the high-T_g side of the interface is relatively muted. This local behavior is consistent with prior reports from our group of the dependence of whole-layer T_g of thinner layered polymers on cross interaction, which

found a crossover from suppression to enhancement of T_g for polymers under hard confinement but not those under soft confinement[35].

As discussed in the introduction, a classical hypothesis for the origins of these types of gradients at polymer-polymer interfaces is a simple local mixing perspective - the idea that the local T_g is controlled by local composition via some mixing rule (either the classical Fox mixing rule or a more advanced model accounting for self-concentration corrections[84]). For example, the Fox mixing rule suggests that T_g is set by composition as

$$1/T_g = w_1/T_{g,1} + w_2/T_{g,2} \qquad (8)$$

where w_1 and w_2 are the weight fractions of species 1 and 2 and $T_{g,1}$ and $T_{g,2}$ are their pure-state T_g's. This type of mixing rule was conceived of at a bulk, mean system level, but is often applied locally in an effort to understand local variations in T_g in compositionally heterogeneous systems. To what extent is T_g within these gradients locally controlled by composition in a manner that might reflect such a scenario?

To begin answering this question, we can first compare these T_g gradients to the data in Figure 1a for local composition gradients in these same systems. This figure provides an initial indication that a local mixing perspective is insufficient: composition gradients can be visually seen to be shorter-ranged than T_g gradients in the same systems. This conclusion becomes even more clear in Figure 1c, where we plot local T_g vs local composition for the same systems shown in Figure 1a. This plot exhibits three features indicating that T_g is not purely locally controlled by composition in a manner that would be consistent with any local mixing scenario, whether accounting for self-concentration effects or not. First, and most minimally, the data do not conform with a local Fox mixing rule; however, from this point alone one might conclude merely that the Fox equation is inadequate; the next two points are more generally dispositive. Second, the local relationship between T_g and composition itself depends strongly on χ. This is in contrast with the basic expectations of a mixing perspective, which anticipate a universal *local* relationship between T_g and composition for these systems at all χ, with differences in T_g gradients driven by χ-dependent variation in the composition gradient breadth. Different mixing rules are expected to differ merely in the form of this expected relationship. Finally, and most definitively, *a large portion of the T_g variation for any system occurs at constant composition* – either within pure low-T_g polymer or pure high-T_g polymer, as indicated by the vertical domains of each data set at the left and right axes. This definitively indicates strong variation of T_g at distances from the interface at which composition gradients are entirely absent – an effect that cannot be accounted for by any composition-based local mixing rule.

In order to understand how a more classical analysis of these gradients in the context of a mixing rule might play out, we show in Figure 4 T_g gradients, composition gradients, and corresponding Fox predictions of T_g gradients from the composition gradients for a pair of representative high-χ and low-χ systems. As can be seen there, generally the composition gradients are appreciably shorter ranged than the T_g gradients, and therefore the Fox mixing rule predictions of the T_g

gradients are qualitatively incorrect. This is consistent with the findings from Figure 1. Figure 4a, however, indicates that the *quantitative* failure of mixing-based approaches will tend to be small for the low-T_g side of the interface in the high-χ limit. This is consistent with Christie et al.'s observation that the Lodge-McLeish mixing rule could describe T_g gradients on the low-T_g side of the interface but not the high T_g side.[32] Figure 4a, however, suggests that this impression simply arises from the fact that T_g-gradients on the low-T_g side can be weak in this case, such that there is little T_g variation for which to account. The inability of mixing rules to predict the T_g behavior more broadly over a range of χ in Figure 1 indicates that a mixing approach does not causally predict the T_g gradient.

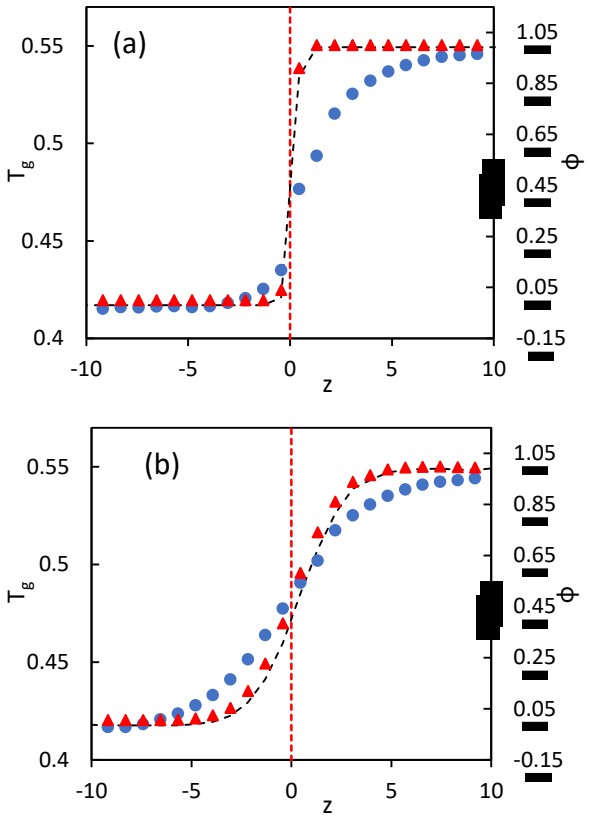

Figure 4. T_g gradient (blue circles), composition gradient (red diamonds), and predicted T_g gradient via the Fox equation and employing local compositions, plotted vs distance from the interface for (a) χ = 1.8 and (b) χ = 0.07.

Does the absence of a general local relationship between T_g and composition indicate that the breadth of composition gradients is irrelevant to the T_g gradient? In order to begin answering this question, we consider several initial measures of the sharpness and breadth of the T_g and composition gradients.

First, we consider a simple measure of inverse sharpness of each gradient *immediately around the interface* - the inverse of the gradient's slope at z = 0. In Figure 5, we plot this quantity for the composition gradient (i.e. $\alpha_\phi = \left(dz/d\phi\right)\big|_{z=0}$) and for the normalized T_g gradient $\Delta T_g/T_g(z)$ (i.e. $\alpha_{T_g} = \Delta T_g \left(dz/dT_g\right)\big|_{z=0}$), where ΔT_g is the difference between the bulk T_g's of the two polymers (the property for the composition gradient is inherently normalized since composition runs from 0 to 1). These ratios report an effective length scale quantifying the breadth of the interface that would be expected if the gradient were linear with slope equal to that observed at z = 0.

As can be seen in Figure 5a, the inverse interfacial sharpness of both composition and T_g gradients depend on χ, with the inverse sharpness of both gradients increasing as χ drops. As shown by Figure 5b, with decreasing log(χ) the T_g inverse sharpness initially grows more rapidly than the composition inverse sharpness. However, as shown by Figure 5c, below $\chi \cong 1$ the difference between α_{Tg} and α_φ becomes much less χ dependent, entering a soft plateau or at least a region

of very weak χ dependence. In this low χ regime, α_{Tg} saturates to the composition inverse sharpness plus a an approximate constant of about $4\sigma_{LJ}$ (about 4 nm in real units):

$$\left.\frac{dz}{dT_g/\Delta T_g}\right|_{z=0} \cong \left.\frac{dz}{d\phi}\right|_{z=0} + 4\sigma_{LJ} \quad \chi_{app} < 1$$

This indicates two things. First, consistent with Figure 1 and Figure 4, this suggests that T_g gradients are appreciably longer ranged than composition gradients such that local T_g cannot be fully locally controlled by local composition. On the other hand, this suggests that at least for low χ (less than about 1 at this molecular weight, but we expect this crossover to be most directly controlled by interfacial composition gradient breadth rather than χ), changes in the interfacial sharpness of T_g gradients track with changes in the interfacial sharpness of composition gradients as χ is varied. In essence, in this regime, broadening of the interfacial composition gradient indeed linearly drives broadening in the T_g gradient.

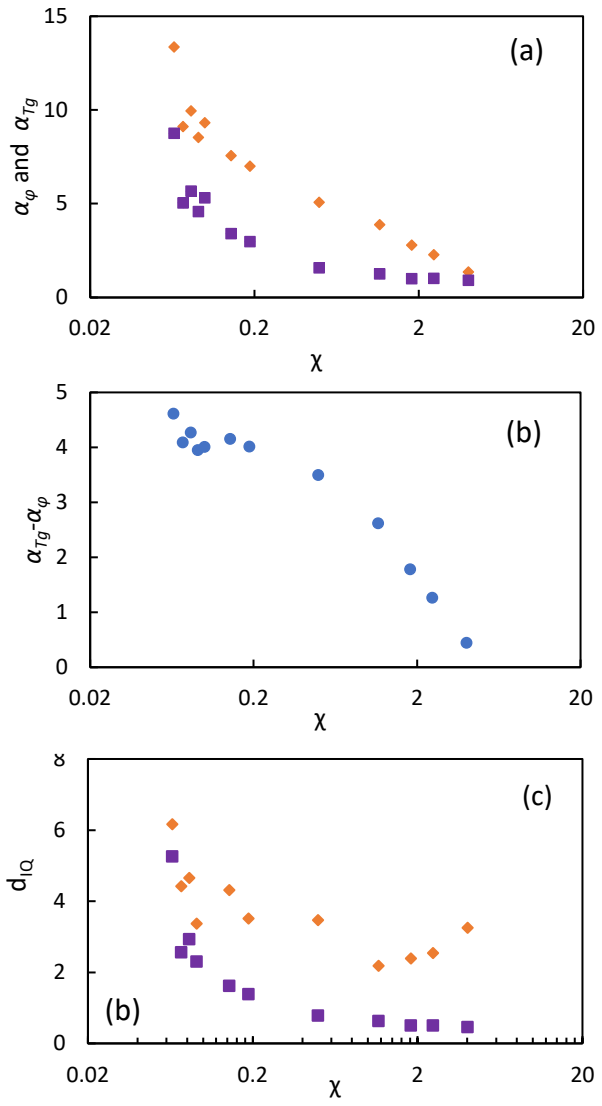

Figure 5. Measures of gradient breadth plotted vs χ. (a) Inverse derivative of normalized T_g with respect to position at the interface (z=0) (orange rhombus) and inverse derivative of composition with respect to position at the interface (z=0) (purple squares). (b) Difference between inverse derivative of composition with respect to position at the interface (z=0) and inverse derivative of glass transition with respect to position at the interface (z=0). (c) Distance between the planes at which the composition (orange triangles) and T_g (purple squares) have traversed 25% and 75% of the difference between their values in the pure low-T_g and high-T_g polymers, as described in the text.

We next consider a measure of the breadth of each gradient over a larger range around the interface (rather than immediately near the interface as in the prior metric): the effective 'interquartile' distance d_{IQ} between the point at which the composition is comprised of 25% low-T_g polymer and the point at which it is comprised of 75% low-T_g polymer. Similarly, we can compute the same quantity for T_g itself by considering the positions at which the gradient has traversed 25% and 75% of the difference between the bulk T_g's of the low-T_g and high-T_g polymers. The results can be seen in Figure 5c. Despite the fact that the ranges in Figure 5a report

on inverse sharpness *near* the interface whereas Figure 5c reports on a breadth across most of the gradient, both exhibit similar qualitative features: d_{IQ} is also consistently larger for T_g than for composition, and the gradients generally grow in range upon reducing χ. The former observation confirms again that the T_g gradient is larger in range than the composition gradient. In this case the difference between d_{IQ} for T_g and φ does not exhibit a clear trend with χ beyond the noise in the data; rather d_{IQ}^{Tg}-d_{IQ}^{φ} is approximately constant at 1.9 ± 0.6 (where the range is the standard deviation over χ) over the χ range. Evidently also by this measure, the range of T_g gradients tracks fairly closely with the range of composition gradients, plus a constant.

These findings are qualitatively consistent with the mix of literature findings above: composition gradients *matter* for T_g gradients, but a local T_g mixing picture does not hold within the gradient.

Gradient asymmetry and range

To better understand the mechanism for this apparently combined thermodynamic/dynamic phenomenon, and to probe its impacts on the features of gradient asymmetry and range discussed above, we now aim to more quantitatively measure the magnitude and range of gradients differentially on either side of the interface. To do so, we first quantify the portion of the overall T_g gradient magnitude that is found on the high-T_g vs low-T_g sides of the interface. The overall T_g difference ΔT_g between the bulk T_gs of the two polymers is equal to 0.132 in reduced LJ temperature units. However, there is no physical requirement that this total change be evenly divided between the two sides of the interface. A local T_g mixing picture would anticipate near symmetry (i.e. a total T_g gradient magnitude of about 0.67 LJ temperature units on either side of the interface), because by definition the segmental mole fraction is 50% at the interface.

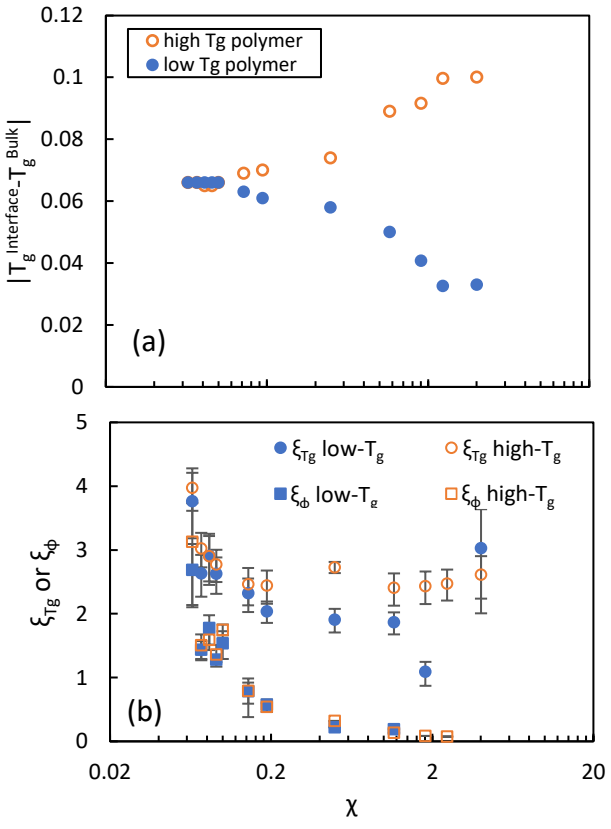

Figure 6. (a) Difference between glass transition temperature at interface and bulk of high-T_g polymer (open orange circle) and low-T_g polymer (closed blue circle). (b) Exponential decay length scale of interfacial T_g gradients temperatures for low-T_g (filled blue circle) and high-T_g (open orange circle) polymers and exponential decay length scale of composition gradients for rubbery (filled blue square) and glassy (open orange square) polymers, all plotted vs. χ. Error bars in part (b) are 95% confidence intervals on the fit parameters.

As can be seen in Figure 6a, the *magnitude* of the T_g gradient is found to be highly asymmetric at high χ, with a larger magnitude gradient on the high-T_g side than the low-T_g side. This is qualitatively consistent with the findings of both Roth and coworkers[34,36,41] and of Christie et al.[32,50], who reported on T_g gradients in layered polymers and block copolymers, respectively, in which the majority of the T_g gradient magnitude is found on the high-T_g side of the interface. Quantitatively, at the highest χ values we simulate we find that the magnitude of the T_g gradient on the high-T_g side is about 3 times that on the low-T_g side. Notably, however, we find that this asymmetry weakens and ultimately vanishes upon approach to the ultra-low-chi limit. For $\chi <$ 0.15 in our simulations, the gradient is evenly divided between the two halves of the interface in terms of magnitude.

We next consider the range of the T_g and composition gradients on either side of the interface. Extensive evidence indicates that T_g gradients at free surfaces obey an exponential gradient form over at least approximately 10 nm near the interface[1,6,57,70,71,85–87]. It is natural to hypothesize that a similar gradient form holds here. Indeed, as shown in Figure 7, we find that the gradients in our simulated systems likewise obey this functional form. This is a finding of considerable interest in its own right, indicating that the dynamical gradient form that is observed at free surfaces also describes dynamics near polymer-polymer interfaces over a wide range of χ. Since the functional form of the gradient is an important signature of the physics governing this gradient[1], this suggests a common mechanism for dynamical gradients near free surfaces and at polymer-polymer interfaces. With this functional form verified, we fit the gradient on either side of the interface to an exponential decay form for each value of χ, and we extract the exponential decay length scale ξ_{Tg}. To extract a consistently defined measure of the range of the composition gradient, we similarly extract composition gradient data at T=0.5 and fit them to an exponential decay form with respect to distance from the interface, with decay constant ξ_ϕ. As shown in Figure 7, the composition gradients can be reasonably well described by an exponential decay to leading order, although not as well as can the T_g gradients. The results of these exponential fits, shown in Figure 6b, reveal several striking features of the interface.

First, the dynamical interface is indeed asymmetric, with the range considerably longer on the high T_g side than the low T_g side. This finding appears to be qualitatively consistent with the experimentally observed T_g gradient asymmetries of Baglay et al.[34,41] and of Christie et al.[50,51] One exception we observe to this asymmetry is at the very highest χ probed, where the low-T_g gradient increases in range to match that of the gradient on the high-T_g side. This occurs because here the value of χ is so high that T_g actually drops with approach to the interface from both sides. Our prior work suggests that this is because there is a density minimum at the interface at these extraordinarily high χ values, such that the interface begins to resemble a free surface[35]. This suggests a general rule that generalizes prior simulation results at free surfaces vs substrates[64,86,87] and is consistent with recent theoretical predictions[88] of the Elastically Collective Nonlinear Langevin Equation Theory of glass formation[89,90] – T_g gradients tend to be somewhat longer-ranged at interfaces where T_g drops than at interfaces where T_g increases relative to bulk. We also note that there appears to be an anomalous drop in the range of the T_g gradient on the

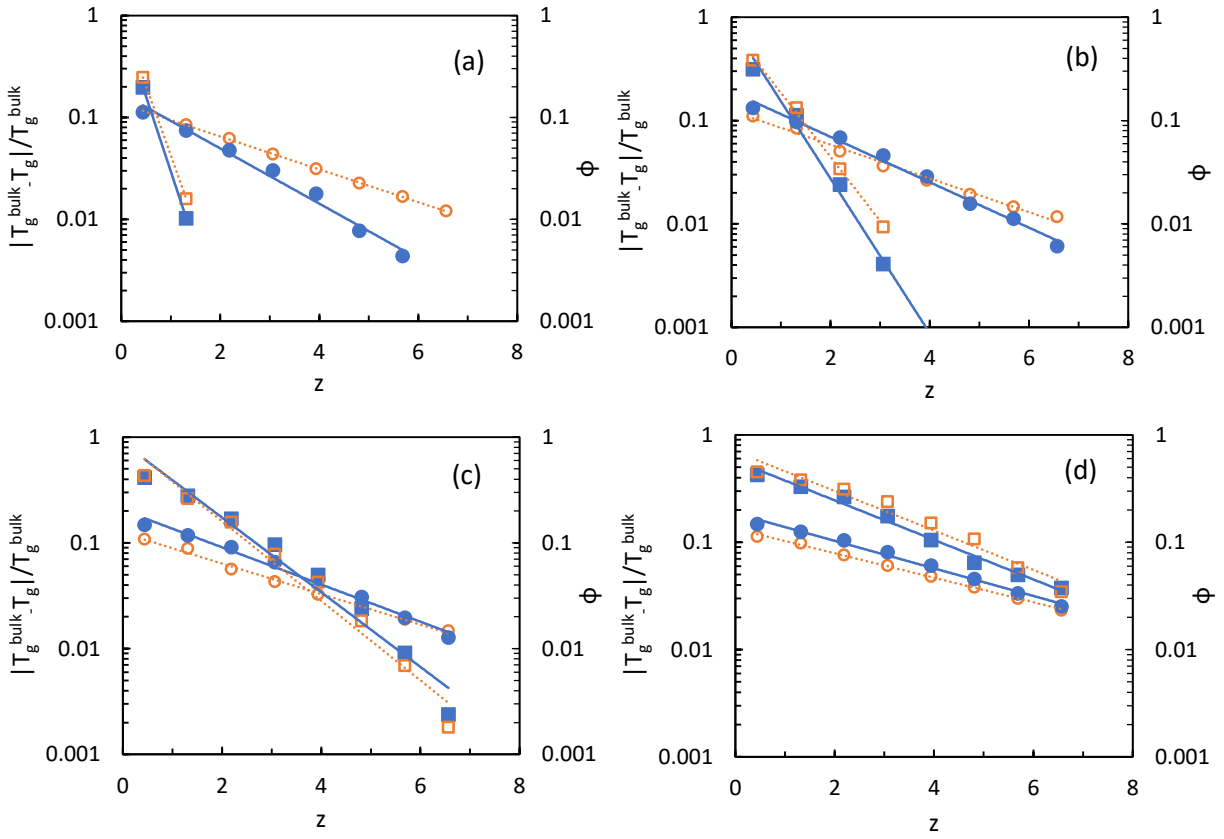

Figure 7. Exponential fits (lines) of glass transition temperature for high-T_g polymer (open orange circles) and composition for high-T_g polymer (open orange squares), and glass transition temperature for low-T_g polymer (filled blue circles) and composition for low-T_g polymer (filled blue squares) (a) for χ = 0.19 , (b) χ =0.14, (c) χ =0.08, (d) $_p$=0.06.

low-Tg side of the interface around χ = 2. This feature is beyond uncertainty, but we have no insight into its origins However, it appears to be localized to a small χ range just short of the compensation condition at which the T_g gradient on the low-χ side vanishes before transitioning from an increasing (at low χ) to a decreasing (at extraordinarily high χ) gradient.

At the same time, Figure 6b indicates that the *composition* gradient is symmetric across the interface across all χ, and that it is several σ_{LJ} (nm) shorter in range than the T_g gradient across all χ. This indicates that the asymmetry in the T_g gradient does not arise due to some underlying thermodynamic gradient asymmetry, but is instead purely dynamical in nature. This would be consistent with prior simulations and theory suggesting that T_g gradients at free surfaces may be generally longer ranged than those at substrates[64,86,87]. The generally longer range of the dynamical gradient than thermodynamic gradients, together with the asymmetry, again emphasizes that local T_g alterations cannot be understood based upon some local mixing rule. This is also consistent with Figure 7, where it is visually clear that T_g gradients are of significantly larger range than composition gradients.

Similar to the findings shown in Figure 5, Figure 6b indicates that the range of both dynamical and thermodynamic gradients grow with decreasing χ. This again emphasizes the finding that, at low χ, the dynamical gradients involve a mixed thermodynamic/dynamic origin, with a broad composition gradient naturally generating a broad dynamical gradient, but dynamical gradients of a purely dynamical origin extending even beyond that. It is also notable that this figure suggests a substantial reduction in the asymmetry of the T_g gradient as χ is reduced to the point at which the innate ranges of the composition and dynamical gradients become comparable – a reasonable result given that the composition gradients are themselves symmetric. This may explain the results of the prior simulation study that reported more symmetric dynamical gradients in a system with a fairly broad interfacial composition gradient[53].

Discussion

The findings above, combined with prior literature, indicate that variations in χ have two distinct effects on dynamical gradients near the interface. First, χ is a proxy for the strength of cross-attractive-interactions, relative to self-interactions, between the two species. Prior works have suggested that the strength of cross interactions at an interface mediates the degree of dynamical coupling across the interface. For example, for a film on a rigid substrate or exposed to a much higher-T_g underlayer, this manifests in the form of larger T_g-enhancements in the presence of stronger cross-attractions[35,66,91]. Here, it can be seen in a more symmetric *magnitude* of T_g alterations on the two sides of the interface as χ is reduced (cross-interactions strengthened).

Second, and distinct from this *magnitude* effect, the presence of thermodynamically broad interfaces enhances the *range* of T_g and dynamical gradients relative to the sharp-gradient (high-χ) limit. This enhancement takes the form of a rough additivity between the range of composition gradients and the innate range of dynamical and T_g gradients. Crucially, here the key variable is almost certainly the range of the composition gradient and not χ directly. Prior field theoretic work has shown that, at low molecular weights, molecular weight variations alter the composition gradient range[55]. At high molecular weights, the composition gradient saturates to a molecular-weight-independent range[55,83]. We thus expect that, for low molecular weights, variations in molecular weight will quantitatively alter the effects observed above even at fixed χ.

The simulations here involve relatively high molecular weights on the scale of simulation, with equation (6) suggesting they should be relatively close to, but not quite at, the high molecular weight limit of composition gradient range. The much higher molecular weights employed in many experiments may thus imply a modestly lower-χ crossover from the high-χ to low-χ gradient regimes reported above than we observe here (reflecting the sharper composition gradients present at the higher molecular weights probed in experiment). This may be relevant to the question of why highly asymmetric gradients have been reported in experiments at high

molecular weight but at relatively low χ, where in our results the asymmetry remains present but is perhaps somewhat muted. We expect more profound effects in simulations and experiments at lower molecular weights, where this transition could be pushed to considerably higher χ.

Perhaps more profoundly, the type of roughly additive range enhancement between composition and dynamical gradients discussed above seemingly cannot account for the extraordinarily long-ranged gradients (>100 nm) reported by Baglay et al.[34,41] However, our findings are qualitatively consistent with a number of other experimental findings. They are consistent with spatially resolved T_g gradients probed in block copolymers, in terms of both the approximate range of the gradient and the asymmetry of the T_g gradient[50,51]. In the high-χ limit, they are consistent with recent measurements of free surface diffusion in small molecules in terms of the range of the dynamical gradient (several nm exponential decay range) and the implied functional form of the gradients (exponential T_g gradients here, double exponential diffusion rate gradients there)[85,92]. This suggests that the difference between our findings and the behavior observed by Baglay et al. is not simply a matter of the time scale accessed by experiment vs simulation.

Moreover, until now it seemed at least plausible that the difference in the ranges probed by Baglay et al. (>100 nm) as compared to Christie et al. (comparable to our findings) was a finite size truncation effect[52] associated with the limited domain sizes accessible in the block copolymers probed there. However, in our present simulations the domain size is considerably larger than twice the exponential gradient range, such that it is not plausible that 'lack of space' is restricting the gradient range. This indicates that domain size limitations alone are not the relevant difference.

Moreover, there are ample historical literature reasons to believe that the range of T_g gradients cannot universally be of order 100 nm at polymer-polymer interfaces. In particular, a long history of measurements of T_g in block copolymers (for example by calorimetry) has often reported on two distinct T_g's in these systems rather than a single broad T_g.[47,93] This ubiquitous observation would not be consistent with the universal presence of 100 nm or more T_g gradients, since domain sizes in block copolymers are well less than that scale. On the other hand, this common experimental block copolymer behavior is entirely consistent with our results. Within our findings, in the limit of high-χ one expects T_g gradients of modest length, with an exponential decay range of 3 nm on the high-T_g side and 1-2 nm on the low-T_g side (with decay of interfacial T_g perturbations by 90% at 2.3 times these distances). This will naturally yield many block copolymers with substantial bulk-like T_g content, even though the interfacial T_g gradient is appreciably broader than the composition gradient. At the same time, it anticipates broadening of T_g's in block copolymers over a range of χ values, which would seem to qualitatively accord with common observations to this effect[43,94]. Indeed, one might expect considerable broadening of the T_g gradient at exceptionally low χ where the composition gradients themselves are exceptionally broad, which could accord with incredibly broad T_g DSC measurements in low-χ block copolymers such as polystyrene-block-poly(alpha-methyl styrene)[95].

All of this leaves open the question of the origin in the disparity between the larger T_g gradient range reported by Baglay et al.[85,92] (and also possibly implied by earlier fluorescence T_g measurements in some high molecular weight films[12]) and the shorter range observed here and in other simulations[31], reported by Christie et al.[32,50] and Li et al.[85] in experiment, and implied by the long history of block copolymer T_g measurements[93]. More recent work by the Roth group has added to this mystery, reporting on very long-ranged T_g gradients near substrates at extremely low grafting densities[96]. We do not have an answer to this question, and indeed in our view it is a significant open question in the field. However, our work combined with prior literature does perhaps narrow the range of plausible explanations. As noted above, neither timescale differences nor finite size effects alone appear to be sufficient to account for the difference.

Another possibility may be that very high molecular weights may play a role, as the use of high molecular weights is fairly standard in the fluorescence measurements used by Roth and coworkers and many others. However, we note that the molecular weights employed here (96-bead chains) appreciably exceed the molecular weights of our prior work in this area (typically 20-bead chains) and are at least modestly over the entanglement molecular weight for these chains, which is reported to be 86 beads[97]. Moreover, these molecular weights are reasonably close to (but not quite at) the high molecular weight limit of the relationship between gradient breadth and χ, as per equation (6). Despite this higher molecular weight, the gradient ranges we report in the extreme high-χ limit (which we have previously shown resemble a free surface as discussed above[35]) are in reasonable agreement with ranges reported in our prior work at those lower molecular weights[68,70,71]. They are also in agreement with other prior simulation work probing the range of these gradients[1,98,99], and with recent experimental work in small molecules[85]. There thus appears to be essentially no growth in the range of the purely dynamical portion of the gradients over a range spanning at least from small molecules to light entanglement. This would not appear to be consistent with a scenario in which the chain scale itself plays some role in amplifying the range of the dynamical portion of the gradients.

On the other hand, depending on how one performs the conversion (on the basis of entanglement molecular weight or Kuhn segment), a 92-bead chain maps to a polystyrene chain on the order of 16,000 to 40,000 g/mol, which is still far below the molecular weights employed by Roth and coworkers. We cannot rule out that some new effect comes into play at extremely high molecular weights in the range of hundreds of thousands, which incidentally is also where a second, molecular-weight-dependent, T_g has been reported in thin films[100]. However, it is of natural interest to ask what possible mechanism could emerge at these high molecular weights of which no hint is observable in the lightly entangled regime. Work by Soyoung and Torkelson has suggested that de Gennes' proposed sliding mechanism[101], which was earlier proposed as a possible mechanism for novel confinement effects at high molecular weights, does not play a role in thin film T_g behavior[36], such that it seems to be an implausible proposition here as well. In equilibrium, an entanglement-based mechanism would seem implausible as well: entanglement is a dynamical rather than structural phenomenon, and it involves timescales much longer than

segmental relaxation, such that the arrow of causality generally points from segmental dynamics to entanglement dynamics, and not the other way around. We are therefore unaware of any viable proposed mechanism by which high molecular weights could lead to a dramatic enhancement in the range of T_g gradients.

Another class of possibilities might center around differences in the quantity being measured here versus in Roth and coworkers' experiments. Here we probe in-equilibrium dynamics and the inferred equilibrium dynamical glass transition temperature. The experiments, on the other hand, probe a pseudo-thermodynamic T_g measured on cooling. There have been suggestions in the literature that there may be intrinsic differences between interface effects on T_g and those on dynamics[102,103]. However, this remains a matter of considerable debate, and the question of whether a gradient in dynamics of range order 10 nm could somehow be consistent with a gradient in pseudo-thermodynamic T_g of order 100 nm is not settled. Nor are differences in the manner in which dynamic and pseudo-thermodynamic measurements weight over local gradients[104] likely to be at work here, since the simulations and several of the key experiments in question are directly reporting local properties.

Recently, Roth and coworkers have suggested that alterations in the propagation of phonon modes across the interface as the composition gradient breadth varies may play a role in yielding the long ranges they observe[52]. However, as they note, the precise mechanism by which this might alter T_g is not clear, and nor is it clear why these proposed effects would be absent from molecular dynamics simulations. In our simulations in particular, the lateral box dimension is comparable to the domain size and the domain size appreciable exceeds the observed gradient range, so that no aphysical finite size truncation of such density waves is expected.

Collectively, the seeming difference between the two sets of T_g gradient ranges observed in the literature at glass-forming interfaces thus remains a major unanswered mystery in the field. One plausible scenario for resolving the seeming quandary summarized above is that a combination of multiple differences involving some of molecular weight, time scale, equilibration state, and perhaps other factors, may be needed to account for this dichotomy if no single factor can alone.

Conclusions

Glass formation behavior at polymer-polymer interfaces is relevant to a wide range of multiphase polymeric systems, including block copolymers, layered polymers, and polymeric adhesives. It is now well established that polymers exhibit a tendency towards gradients in T_g and dynamics over a range exceeding typical gradients in structure, thermodynamics, and composition. Here, we employ simulations to understand how this tendency towards long-ranged gradients plays out in the presence of the broad (and χ-dependent) composition gradients present at polymer-polymer interfaces. Our results point to a transition from purely dynamical T_g gradients in the high-χ limit to a mixed composition/dynamical gradient at lower χ. In this latter case, the ranges of the composition and dynamical contributions to the gradient appear to be nearly additive. Consistent

with experiment, the T_g gradient is found to be asymmetric, with longer ranged effects on the high-T_g side than the low-T_g side of the gradient. This type of asymmetry – longer-ranged T_g gradients at soft interfaces than hard interfaces – was predicted in 2013 by Tito et al based upon a kinetic lattice model[105]. More recently, it has been predicted by the Elastically Collective Nonlinear Langevin Equation Theory of glass formation[89,90], which has been shown to predict numerous features of the altered dynamics observed near free surfaces and substrates[1,72,88,106]. There, this behavior emerges as a consequence of the combination of caging and long-ranged elastic effects that underlie that theory[88].

This behavior may be of considerable relevance to the design of block copolymers for applications such as next generation ion conductors and block copolymer membranes, where an understanding of the profile of mobility within the domains is of particular importance in mediating transport behavior.[107–110] The dynamical gradient effect we report above is expected to be of pronounced importance in the strong and intermediate segregation regimes, where our results suggest that T_g gradients will extend over a longer range than composition gradients. In effect, it may be possible for a block copolymer system to be in a weak 'T_g segregation regime' while being in an intermediate or strong 'composition segregation regime'. This observation may bear on the interpretation of DSC measurements in block copolymer systems, for example. On the other hand, block copolymers in the weak segregation limit, where the interfacial composition gradient extends essentially through the full domain, logically cannot exhibit a longer ranged dynamical gradient than composition gradient, because there is no available space. However, the results above suggest that one should expect larger local T_g variations in these systems than would be expected from local composition mixing effects alone, due to the combined thermodynamic/dynamic origin of T_g gradients under these circumstances. This type of effect is likely to be subtle, but it may be significant in influencing transport rates in weakly segregated block copolymer domains.

The gradient asymmetry observed here is also of considerable potential importance to the design of block copolymers for transport applications. Enhancements in the T_g of a rubbery domain in a rubbery/glassy block copolymer can play an adverse role in performance, reducing transport rates and thus impeding ion mobility (exe. in polymeric electrolytes for battery applications) or permeability[108–110]. Conversely, suppressions in the T_g on the high-T_g side in these systems can conversely impact mechanical properties, as the glassy domain is generally intended to maintain mechanical cohesion or establish a high modulus on the macrosale. Our findings of a generally larger range on the high-T_g side, which accord qualitatively with experiment, thus may suggest that modestly larger block lengths are needed on glassy than on rubbery sides to ensure the presence of a bulk-like region within each microphase separated domain.

Indeed, our data in Figure 6 allow for an approximate estimate of the domain sizes necessary to ensure that a bulk-like T_g domain is present in each domain type. While an exact conversion from the length scales we observe in simulation to experimental values is not possible, standard conversions and comparison with the experimental gradient data of Li et al[85] suggest a

conversion of approximately 1 bead diameter to 1 nm. One reasonable measure for recovery of a bulk-like region in the mid-film is the domain size for which 90% of the interfacial T_g perturbation decays by the domain midline. Employing this convention, the range data in Figure 6 suggest that for high-χ systems a region of bulklike T_g should be recovered around a ~15 nm domain size on the high-T_g side and ~6-9 nm on the low-T_g side. With decreasing χ, our data suggest that the required domain size for recovery of bulk regions grows, with Figure 6 suggesting that at the lowest χ value we probe domain sizes of ~23 nm and ~20 nm are required on the high- and low-T_g sides, respectively, to ensure that a region of bulk-like T_g is present along the domain midline. We note that in interpreting these values, it is essential to account for the fact that distinct T_g metrologies (exe. dynamic scanning calorimetry vs dielectric spectroscopy) average differently over these local gradients[67,104,111–121], such that the precise thickness for which bulk-like T_g behavior dominates will be metrology dependent.

We note that the literature appears to reflect a dichotomy of reported length scales for T_g gradients, with simulation studies[65–67,70,71,86,87], studies in small molecules[92], and studies in most block copolymers[51,93] suggesting ranges that seem consistent with those we find here. On the other hand, another set of studies in high molecular weight polymers, and usually employing fluorescence T_g measurements, have pointed towards considerably longer length scales[8] (on the order of many tens or perhaps hundreds of nm) at high molecular weights near polymer-polymer interfaces[34,41], lightly grafted substrates[96], and possibly in supported films[12]. We suggest that this dichotomy, which to our knowledge remains unexplained, is one of the major open questions in this field. However, our results combined with literature data likely rule out several possible explanations. We find that simple thermodynamic broadening of the interface does not sufficiently amplify the T_g gradient range to account for the larger-ranged set of results. Our box is large enough to rule out a simple finite-domain-size truncation of the gradient range[54], such that differences in domain sizes of block copolymers (in the smaller reported range set) vs thick layered polymers (in the larger reported range set) are not on their own a likely explanation. Accordance of our simulated ranges with those reported in experiment by Li et al[85] and by Christie et al.[51] rule out simulation timescale limitations as a sole cause of the difference. It seems plausible that a combination of differences rather than a single factor may be necessary to account for these two distinct datasets. We expect that highly targeted simulations and experiments will be necessary to resolve this major remaining open question.

Acknowledgements

This material is based upon work supported by the National Science Foundation under Grant No. CBET – 2208238. The authors acknowledge helpful discussions with and feedback from Dr. Connie Roth.

References

(1) Schweizer, K. S.; Simmons, D. S. Progress towards a Phenomenological Picture and Theoretical Understanding of Glassy Dynamics and Vitrification near Interfaces and under Nanoconfinement. *Journal of Chemical Physics* **2019**, *151*, 240901.

(2) Jackson, C. L.; McKenna, G. B. Vitrification and Crystallization of Organic Liquids Confined to Nanoscale Pores. *Chem. Mater.* **1996**, *8* (8), 2128–2137. https://doi.org/10.1021/cm9601188.

(3) Ediger, M. D.; Forrest, J. A. Dynamics near Free Surfaces and the Glass Transition in Thin Polymer Films: A View to the Future. *Macromolecules* **2014**, *47* (2), 471–478. https://doi.org/10.1021/ma4017696.

(4) Richert, R. Dynamics of Nanoconfined Supercooled Liquids. *Annual Review of Physical Chemistry* **2011**, *62* (1), 65–84. https://doi.org/10.1146/annurev-physchem-032210-103343.

(5) McKenna, G. B. Ten (or More) Years of Dynamics in Confinement: Perspectives for 2010. *Eur. Phys. J. Spec. Top.* **2010**, *189* (1), 285–302. https://doi.org/10.1140/epjst/e2010-01334-8.

(6) Baschnagel, J.; Varnik, F. Computer Simulations of Supercooled Polymer Melts in the Bulk and in Confined Geometry. *Journal of Physics: Condensed Matter* **2005**, *17* (32), R851–R953. https://doi.org/10.1088/0953-8984/17/32/R02.

(7) Forrest, J. A.; Dalnoki-Veress, K. The Glass Transition in Thin Polymer Films. *Advances in Colloid and Interface Science* **2001**, *94* (1–3), 167–195. https://doi.org/10.1016/S0001-8686(01)00060-4.

(8) B. Roth, C. Polymers under Nanoconfinement: Where Are We Now in Understanding Local Property Changes? *Chemical Society Reviews* **2021**, *50* (14), 8050–8066. https://doi.org/10.1039/D1CS00054C.

(9) Simmons, D. S. An Emerging Unified View of Dynamic Interphases in Polymers. *Macromol. Chem. Phys.* **2016**, *217* (2), 137–148. https://doi.org/10.1002/macp.201500284.

(10) Forrest, J.; Dalnoki-Veress, K.; Dutcher, J. Interface and Chain Confinement Effects on the Glass Transition Temperature of Thin Polymer Films. *Physical Review E* **1997**, *56*, 5705–5716. https://doi.org/10.1103/PhysRevE.56.5705.

(11) Keddie, J. L.; Jones, R. A. L.; Cory, R. A. Size-Dependent Depression of the Glass Transition Temperature in Polymer Films. *Europhysics Letters (EPL)* **1994**, *27*, 59–64. https://doi.org/10.1209/0295-5075/27/1/011.

(12) Ellison, C. J.; Torkelson, J. M. The Distribution of Glass-Transition Temperatures in Nanoscopically Confined Glass Formers. *Nature Materials* **2003**, *2* (10), 695–700. https://doi.org/10.1038/nmat980.

(13) Fukao, K.; Miyamoto, Y. Slow Dynamics near Glass Transitions in Thin Polymer Films. *Phys. Rev. E* **2001**, *64* (1), 011803. https://doi.org/10.1103/PhysRevE.64.011803.

(14) Fakhraai, Z.; Forrest, J. A. Probing Slow Dynamics in Supported Thin Polymer Films. *Phys. Rev. Lett.* **2005**, *95* (2), 025701. https://doi.org/10.1103/PhysRevLett.95.025701.

(15) Fakhraai, Z.; Forrest, J. A. Measuring the Surface Dynamics of Glassy Polymers. *Science* **2008**, *319* (5863), 600–604. https://doi.org/10.1126/science.1151205.

(16) Varnik, F.; Baschnagel, J.; Binder, K. Reduction of the Glass Transition Temperature in Polymer Films: A Molecular-Dynamics Study. *Phys. Rev. E* **2002**, *65* (2), 021507. https://doi.org/10.1103/PhysRevE.65.021507.

(17) Lee, J.; Mangalara, J. H.; Simmons, D. S. Correspondence between the Rigid Amorphous Fraction and Nanoconfinement Effects on Glass Formation. *J. Polym. Sci. Part B: Polym. Phys.* **2017**, *55* (12), 907–918. https://doi.org/10.1002/polb.24324.

(18) Wunderlich, B. Reversible Crystallization and the Rigid-Amorphous Phase in Semicrystalline Macromolecules. *Prog. Polym. Sci.* **2003**, *28* (3), 383–450. https://doi.org/10.1016/S0079-6700(02)00085-0.

(19) Zia, Q.; Mileva, D.; Androsch, R. Rigid Amorphous Fraction in Isotactic Polypropylene. *Macromolecules* **2008**, *41* (21), 8095–8102. https://doi.org/10.1021/ma801455m.
(20) Ma, Q.; Georgiev, G.; Cebe, P. Constraints in Semicrystalline Polymers: Using Quasi-Isothermal Analysis to Investigate the Mechanisms of Formation and Loss of the Rigid Amorphous Fraction. *Polymer* **2011**, *52* (20), 4562–4570.
(21) Aharoni, S. M. Increased Glass Transition Temperature in Motionally Constrained Semicrystalline Polymers. *Polym. Adv. Technol.* **1998**, *9* (3), 169–201. https://doi.org/10.1002/(SICI)1099-1581(199803)9:3<169::AID-PAT740>3.3.CO;2-Q.
(22) Bansal, A.; Yang, H.; Li, C.; Cho, K.; Benicewicz, B. C.; Kumar, S. K.; Schadler, L. S. Quantitative Equivalence between Polymer Nanocomposites and Thin Polymer Films. *Nat Mater* **2005**, *4* (9), 693–698. https://doi.org/10.1038/nmat1447.
(23) Betancourt, B. A. P.; Douglas, J. F.; Starr, F. W. Fragility and Cooperative Motion in a Glass-Forming Polymer–Nanoparticle Composite. *Soft Matter* **2012**, *9* (1), 241–254. https://doi.org/10.1039/C2SM26800K.
(24) Carroll, B.; Cheng, S.; Sokolov, A. P. Analyzing the Interfacial Layer Properties in Polymer Nanocomposites by Broadband Dielectric Spectroscopy. *Macromolecules* **2017**, *50* (16), 6149–6163. https://doi.org/10.1021/acs.macromol.7b00825.
(25) Ruan, D.; Simmons, D. S. Glass Formation near Covalently Grafted Interfaces: Ionomers as a Model Case. *Macromolecules* **2015**, *48* (7), 2313–2323. https://doi.org/10.1021/acs.macromol.5b00025.
(26) Ruan, D.; Simmons, D. S. Roles of Chain Stiffness and Segmental Rattling in Ionomer Glass Formation. *Journal of Polymer Science Part B: Polymer Physics* **2015**, *53* (20), 1458–1469. https://doi.org/10.1002/polb.23788.
(27) Eisenberg, A.; Hird, B.; Moore, R. B. A New Multiplet-Cluster Model for the Morphology of Random Ionomers. *Macromolecules* **1990**, *23* (18), 4098–4107. https://doi.org/10.1021/ma00220a012.
(28) Weiss, R.; Fitzgerald, J.; Kim, D. Viscoelastic Behavior of Lightly Sulfonated Polystyrene Ionomers. *Macromolecules* **1991**, *24* (5), 1071–1076. https://doi.org/10.1021/ma00005a015.
(29) Buitrago, C. F.; Bolintineanu, D. S.; Seitz, M. E.; Opper, K. L.; Wagener, K. B.; Stevens, M. J.; Frischknecht, A. L.; Winey, K. I. Direct Comparisons of X-Ray Scattering and Atomistic Molecular Dynamics Simulations for Precise Acid Copolymers and Ionomers. *Macromolecules* **2015**, *48* (4), 1210–1220. https://doi.org/10.1021/ma5022117.
(30) Choi, U. H.; Middleton, L. R.; Soccio, M.; Buitrago, C. F.; Aitken, B. S.; Masser, H.; Wagener, K. B.; Winey, K. I.; Runt, J. Dynamics of Precise Ethylene Ionomers Containing Ionic Liquid Functionality. *Macromolecules* **2015**, *48* (2), 410–420. https://doi.org/10.1021/ma502168e.
(31) Slimani, M. Z.; Moreno, A. J.; Colmenero, J. Heterogeneity of the Segmental Dynamics in Lamellar Phases of Diblock Copolymers. *Macromolecules* **2011**, *44* (17), 6952–6961. https://doi.org/10.1021/ma200470a.
(32) Christie, D.; Register, R. A.; Priestley, R. D. Direct Measurement of the Local Glass Transition in Self-Assembled Copolymers with Nanometer Resolution. *ACS Cent. Sci.* **2018**, *4* (4), 504–511. https://doi.org/10.1021/acscentsci.8b00043.
(33) Roth, C. B.; Torkelson, J. M. Selectively Probing the Glass Transition Temperature in Multilayer Polymer Films: Equivalence of Block Copolymers and Multilayer Films of Different Homopolymers. *Macromolecules* **2007**, *40* (9), 3328–3336. https://doi.org/10.1021/ma070162g.
(34) Baglay, R. R.; Roth, C. B. Communication: Experimentally Determined Profile of Local Glass Transition Temperature across a Glassy-Rubbery Polymer Interface with a Tg Difference of 80 K. *The Journal of Chemical Physics* **2015**, *143* (11), 111101. https://doi.org/10.1063/1.4931403.

(35) Lang, R. J.; Merling, W. L.; Simmons, D. S. Combined Dependence of Nanoconfined Tg on Interfacial Energy and Softness of Confinement. *ACS Macro Lett.* **2014**, *3*, 758–762. https://doi.org/10.1021/mz500361v.

(36) Evans, C. M.; Kim, S.; Roth, C. B.; Priestley, R. D.; Broadbelt, L. J.; Torkelson, J. M. Role of Neighboring Domains in Determining the Magnitude and Direction of Tg-Confinement Effects in Binary, Immiscible Polymer Systems. *Polymer* **2015**, *80*, 180–187. https://doi.org/10.1016/j.polymer.2015.10.059.

(37) Arabeche, K.; Delbreilh, L.; Saiter, J.-M.; Michler, G. H.; Adhikari, R.; Baer, E. Fragility and Molecular Mobility in Micro- and Nano-Layered PC/PMMA Films. *Polymer* **2014**, *55* (6), 1546–1551. https://doi.org/10.1016/j.polymer.2014.02.006.

(38) Koh, Y. P.; Simon, S. L. Structural Relaxation of Stacked Ultrathin Polystyrene Films. *Journal of Polymer Science Part B: Polymer Physics* **2008**, *46* (24), 2741–2753. https://doi.org/10.1002/polb.21598.

(39) Slimani, M. Z.; Moreno, A. J.; Colmenero, J. Heterogeneity of the Segmental Dynamics in Cylindrical and Spherical Phases of Diblock Copolymers. *Macromolecules* **2012**, *45* (21), 8841–8852. https://doi.org/10.1021/ma301388j.

(40) Slimani, M. Z.; Moreno, A. J.; Rossi, G.; Colmenero, J. Dynamic Heterogeneity in Random and Gradient Copolymers: A Computational Investigation. *Macromolecules* **2013**, *46* (12), 5066–5079. https://doi.org/10.1021/ma400577d.

(41) Baglay, R. R.; Roth, C. B. Local Glass Transition Temperature $T_g(z)$ of Polystyrene next to Different Polymers: Hard vs. Soft Confinement. *The Journal of Chemical Physics* **2017**, *146* (20), 203307. https://doi.org/10.1063/1.4975168.

(42) Evans, C. M.; Sandoval, R. W.; Torkelson, J. M. Glass Transition Temperature of a Component near Infinite Dilution in Binary Polymer Blends: Determination via Fluorescence Spectroscopy. *Macromolecules* **2011**, *44* (17), 6645–6648. https://doi.org/10.1021/ma201259w.

(43) Robertson, C. G.; Hogan, T. E.; Rackaitis, M.; Puskas, J. E.; Wang, X. Effect of Nanoscale Confinement on Glass Transition of Polystyrene Domains from Self-Assembly of Block Copolymers. *J Chem Phys* **2010**, *132* (10), 104904. https://doi.org/10.1063/1.3337910.

(44) Mok, M.; Kim, J.; Marrou, S.; Torkelson, J. Ellipsometry Measurements of Glass Transition Breadth in Bulk Films of Random, Block, and Gradient Copolymers. *The European Physical Journal E: Soft Matter and Biological Physics* **2010**, *31* (3), 239–252. https://doi.org/10.1140/epje/i2010-10569-3.

(45) Mok, M. M.; Masser, K. A.; Runt, J.; Torkelson, J. M. Dielectric Relaxation Spectroscopy of Gradient Copolymers and Block Copolymers: Comparison of Breadths in Relaxation Time for Systems with Increasing Interphase. *Macromolecules* **2010**, *43* (13), 5740–5748. https://doi.org/10.1021/ma100743s.

(46) Wong, C. L. H.; Kim, J.; Torkelson, J. M. Breadth of Glass Transition Temperature in Styrene/Acrylic Acid Block, Random, and Gradient Copolymers: Unusual Sequence Distribution Effects. *Journal of Polymer Science Part B: Polymer Physics* **2007**, *45* (20), 2842–2849. https://doi.org/10.1002/polb.21296.

(47) Kim, J.; Mok, M. M.; Sandoval, R. W.; Woo, D. J.; Torkelson, J. M. Uniquely Broad Glass Transition Temperatures of Gradient Copolymers Relative to Random and Block Copolymers Containing Repulsive Comonomers. *Macromolecules* **2006**, *39* (18), 6152–6160. https://doi.org/10.1021/ma061241f.

(48) Bares, J. Glass Transition of the Polymer Microphase. *Macromolecules* **1975**, *8* (2), 244–246. https://doi.org/10.1021/ma60044a030.

(49) Arabeche, K.; Delbreilh, L.; Adhikari, R.; Michler, G. H.; Hiltner, A.; Baer, E.; Saiter, J.-M. Study of the Cooperativity at the Glass Transition Temperature in PC/PMMA Multilayered Films: Influence

of Thickness Reduction from Macro- to Nanoscale. *Polymer* **2012**, *53* (6), 1355–1361. https://doi.org/10.1016/j.polymer.2012.01.045.

(50) Christie, D.; Register, R. A.; Priestley, R. D. Role of Chain Connectivity across an Interface on the Dynamics of a Nanostructured Block Copolymer. *Phys. Rev. Lett.* **2018**, *121* (24), 247801. https://doi.org/10.1103/PhysRevLett.121.247801.

(51) Christie, D.; Register, R. A.; Priestley, R. D. Direct Measurement of the Local Glass Transition in Self-Assembled Copolymers with Nanometer Resolution. *ACS Cent. Sci.* **2018**, *4* (4), 504–511. https://doi.org/10.1021/acscentsci.8b00043.

(52) Gagnon, Y. J.; Roth, C. B. Local Glass Transition Temperature Tg(z) Within Polystyrene Is Strongly Impacted by the Modulus of the Neighboring PDMS Domain. *ACS Macro Lett.* **2020**, *9* (11), 1625–1631. https://doi.org/10.1021/acsmacrolett.0c00659.

(53) Hsu, D. D.; Xia, W.; Song, J.; Keten, S. Dynamics of Interacting Interphases in Polymer Bilayer Thin Films. *MRS Communications* **2017**, *7* (4), 832–839. https://doi.org/10.1557/mrc.2017.113.

(54) Baglay, R. R.; Roth, C. B. Experimental Study of the Influence of Periodic Boundary Conditions: Effects of Finite Size and Faster Cooling Rates on Dissimilar Polymer–Polymer Interfaces. *ACS Macro Lett.* **2017**, *6* (8), 887–891. https://doi.org/10.1021/acsmacrolett.7b00485.

(55) Broseta, D.; Fredrickson, G. H.; Helfand, E.; Leibler, L. Molecular Weight and Polydispersity Effects at Polymer-Polymer Interfaces. *Macromolecules* **1990**, *23* (1), 132–139.

(56) Mackura, M. E.; Simmons, D. S. Enhancing Heterogenous Crystallization Resistance in a Bead-Spring Polymer Model by Modifying Bond Length. *Journal of Polymer Science Part B: Polymer Physics* **2014**, *52* (2), 134–140. https://doi.org/10.1002/polb.23398.

(57) Peter, S.; Meyer, H.; Baschnagel, J.; Seemann, R. Slow Dynamics and Glass Transition in Simulated Free-Standing Polymer Films: A Possible Relation between Global and Local Glass Transition Temperatures. *J. Phys.-Condes. Matter* **2007**, *19* (20), 205119. https://doi.org/10.1088/0953-8984/19/20/205119.

(58) Torres, J. A.; Nealey, P. F.; de Pablo, J. J. Molecular Simulation of Ultrathin Polymeric Films near the Glass Transition. *Phys. Rev. Lett.* **2000**, *85* (15), 3221–3224. https://doi.org/10.1103/PhysRevLett.85.3221.

(59) Jain, T. S.; de Pablo, J. J. Investigation of Transition States in Bulk and Freestanding Film Polymer Glasses. *Phys. Rev. Lett.* **2004**, *92* (15), 155505.

(60) Riggleman, R. A.; Yoshimoto, K.; Douglas, J. F.; de Pablo, J. J. Influence of Confinement on the Fragility of Antiplasticized and Pure Polymers. *Phys. Rev. Lett.* **2006**, *97*, 0455021–0455024.

(61) Shavit, A.; Riggleman, R. A. Physical Aging, the Local Dynamics of Glass-Forming Polymers under Nanoscale Confinement. *J. Phys. Chem. B* **2014**, *118* (30), 9096–9103. https://doi.org/10.1021/jp502952n.

(62) Shavit, A.; Riggleman, R. A. Influence of Backbone Rigidity on Nanoscale Confinement Effects in Model Glass-Forming Polymers. *Macromolecules* **2013**, *46*, 5044–5052. https://doi.org/10.1021/ma400210w.

(63) Ivancic, R. J. S.; Riggleman, R. A. Dynamic Phase Transitions in Freestanding Polymer Thin Films. *PNAS* **2020**, *117* (41), 25407–25413. https://doi.org/10.1073/pnas.2006703117.

(64) Hanakata, P. Z.; Douglas, J. F.; Starr, F. W. Local Variation of Fragility and Glass Transition Temperature of Ultra-Thin Supported Polymer Films. *The Journal of Chemical Physics* **2012**, *137* (24), 244901. https://doi.org/doi:10.1063/1.4772402.

(65) Hanakata, P. Z.; Douglas, J. F.; Starr, F. W. Interfacial Mobility Scale Determines the Scale of Collective Motion and Relaxation Rate in Polymer Films. *Nature Communications* **2014**, *5*, 4163. https://doi.org/10.1038/ncomms5163.

(66) Hanakata, P. Z.; Betancourt, B. A. P.; Douglas, J. F.; Starr, F. W. A Unifying Framework to Quantify the Effects of Substrate Interactions, Stiffness, and Roughness on the Dynamics of Thin Supported

Polymer Films. *The Journal of Chemical Physics* **2015**, *142* (23), 234907. https://doi.org/10.1063/1.4922481.

(67) Lang, R. J.; Simmons, D. S. Interfacial Dynamic Length Scales in the Glass Transition of a Model Freestanding Polymer Film and Their Connection to Cooperative Motion. *Macromolecules* **2013**, *46* (24), 9818–9825. https://doi.org/10.1021/ma401525q.

(68) Mangalara, J. H.; Marvin, M. D.; Wiener, N. R.; Mackura, M. E.; Simmons, D. S. Does Fragility of Glass Formation Determine the Strength of Tg-Nanoconfinement Effects? *The Journal of Chemical Physics* **2017**, *146* (10), 104902. https://doi.org/10.1063/1.4976521.

(69) Chowdhury, M.; Guo, Y.; Wang, Y.; Merling, W. L.; Mangalara, J. H.; Simmons, D. S.; Priestley, R. D. Spatially Distributed Rheological Properties in Confined Polymers by Noncontact Shear. *J. Phys. Chem. Lett.* **2017**, 1229–1234. https://doi.org/10.1021/acs.jpclett.7b00214.

(70) Vela, D.; Ghanekarade, A.; Simmons, D. S. Probing the Metrology and Chemistry Dependences of the Onset Condition of Strong "Nanoconfinement" Effects on Dynamics. *Macromolecules* **2020**, *53* (11), 4158–4171. https://doi.org/10.1021/acs.macromol.9b02693.

(71) Diaz-Vela, D.; Hung, J.-H.; Simmons, D. S. Temperature-Independent Rescaling of the Local Activation Barrier Drives Free Surface Nanoconfinement Effects on Segmental-Scale Translational Dynamics near Tg. *ACS Macro Lett.* **2018**, 1295–1301. https://doi.org/10.1021/acsmacrolett.8b00695.

(72) Ghanekarade, A.; Phan, A. D.; Schweizer, K. S.; Simmons, D. S. Nature of Dynamic Gradients, Glass Formation, and Collective Effects in Ultrathin Freestanding Films. *PNAS* **2021**, *118* (31), e2104398118. https://doi.org/10.1073/pnas.2104398118.

(73) Xu, W.-S.; Douglas, J. F.; Freed, K. F. Influence of Cohesive Energy on Relaxation in a Model Glass-Forming Polymer Melt. *Macromolecules* **2016**, *49* (21), 8355–8370. https://doi.org/10.1021/acs.macromol.6b01504.

(74) Plimpton, S. J. Fast Parallel Algorithms for Short-Range Molecular Dynamics. *J. Comp. Phys.* **1995**, *117*, 1–19.

(75) Martínez, L.; Andrade, R.; Birgin, E. G.; Martínez, J. M. PACKMOL: A Package for Building Initial Configurations for Molecular Dynamics Simulations. *Journal of Computational Chemistry* **2009**, *30* (13), 2157–2164. https://doi.org/10.1002/jcc.21224.

(76) Hung, J.-H.; Mangalara, J. H.; Simmons, D. S. Heterogeneous Rouse Model Predicts Polymer Chain Translational Normal Mode Decoupling. *Macromolecules* **2018**, *51* (8), 2887–2898. https://doi.org/10.1021/acs.macromol.8b00135.

(77) Rahman, T.; Simmons, D. S. Near-Substrate Gradients in Chain Relaxation and Viscosity in a Model Low-Molecular Weight Polymer. *Macromolecules* **2021**, *54* (13), 5935–5949. https://doi.org/10.1021/acs.macromol.0c02888.

(78) Vogel, H. Das Temperatur-Abhängigkeitsgesetz Der Viskosität von Flüssigkeiten. *Phys. Zeit.* **1921**, *22*, 645–646.

(79) Fulcher, G. S. Analysis of Recent Measurements of the Viscosity of Glasses. *J. Am. Ceram. Soc.* **1925**, *8*, 339.

(80) Xia, W.; Hsu, D. D.; Keten, S. Molecular Weight Effects on the Glass Transition and Confinement Behavior of Polymer Thin Films. *Macromol. Rapid Commun.* **2015**, *36* (15), 1422–1427. https://doi.org/10.1002/marc.201500194.

(81) Hsu, D. D.; Xia, W.; Song, J.; Keten, S. Glass-Transition and Side-Chain Dynamics in Thin Films: Explaining Dissimilar Free Surface Effects for Polystyrene vs Poly(Methyl Methacrylate). *ACS Macro Lett.* **2016**, *5* (4), 481–486. https://doi.org/10.1021/acsmacrolett.6b00037.

(82) Meenakshisundaram, V.; Hung, J.-H.; Simmons, D. S. Design Rules for Glass Formation from Model Molecules Designed by a Neural-Network-Biased Genetic Algorithm. *Soft Matter* **2019**, *15*, 7795–7808. https://doi.org/10.1039/C9SM01486A.

(83) Semenov, A. N. Theory of Block Copolymer Interfaces in the Strong Segregation Limit. *Macromolecules* **1993**, *26* (24), 6617–6621. https://doi.org/10.1021/ma00076a047.
(84) Lodge, T. P.; McLeish, T. C. B. Self-Concentrations and Effective Glass Transition Temperatures in Polymer Blends. *Macromolecules* **2000**, *33* (14), 5278–5284. https://doi.org/10.1021/ma9921706.
(85) Li, Y.; Zhang, W.; Bishop, C.; Huang, C.; Ediger, M. D.; Yu, L. Surface Diffusion in Glasses of Rod-like Molecules Posaconazole and Itraconazole: Effect of Interfacial Molecular Alignment and Bulk Penetration. *Soft Matter* **2020**, *16* (21), 5062–5070. https://doi.org/10.1039/D0SM00353K.
(86) Scheidler, P.; Kob, W.; Binder, K. Cooperative Motion and Growing Length Scales in Supercooled Confined Liquids. *Europhys. Lett.* **2002**, *59* (5), 701–707. https://doi.org/10.1209/epl/i2002-00182-9.
(87) Scheidler, P.; Kob, W.; Binder, K. The Relaxation Dynamics of a Supercooled Liquid Confined by Rough Walls. *J. Phys. Chem. B* **2004**, *108* (21), 6673–6686. https://doi.org/10.1021/jp036593s.
(88) Phan, A. D.; Schweizer, K. S. Theory of Spatial Gradients of Relaxation, Vitrification Temperature and Fragility of Glass-Forming Polymer Liquids Near Solid Substrates. *ACS Macro Lett.* **2020**, *9* (4), 448–453. https://doi.org/10.1021/acsmacrolett.0c00006.
(89) Mirigian, S.; Schweizer, K. S. Elastically Cooperative Activated Barrier Hopping Theory of Relaxation in Viscous Fluids. I. General Formulation and Application to Hard Sphere Fluids. *J. Chem. Phys.* **2014**, *140* (19), 194506. https://doi.org/10.1063/1.4874842.
(90) Mirigian, S.; Schweizer, K. S. Elastically Cooperative Activated Barrier Hopping Theory of Relaxation in Viscous Fluids. II. Thermal Liquids. *J. Chem. Phys.* **2014**, *140* (19), 194507. https://doi.org/10.1063/1.4874843.
(91) Merling, W. L.; Mileski, J. B.; Douglas, J. F.; Simmons, D. S. The Glass Transition of a Single Macromolecule. *Macromolecules* **2016**, *49* (19), 7597–7604. https://doi.org/10.1021/acs.macromol.6b01461.
(92) Li, Y.; Annamareddy, A.; Morgan, D.; Yu, Z.; Wang, B.; Cao, C.; Perepezko, J. H.; Ediger, M. D.; Voyles, P. M.; Yu, L. Surface Diffusion Is Controlled by Bulk Fragility across All Glass Types. *Phys. Rev. Lett.* **2022**, *128* (7), 075501. https://doi.org/10.1103/PhysRevLett.128.075501.
(93) Angelo, R. J.; Ikeda, R. M.; Wallach, M. L. Multiple Glass Transitions of Block Polymers. *Polymer* **1965**, *6* (3), 141–156. https://doi.org/10.1016/0032-3861(65)90003-0.
(94) Rosati, D.; Perrin, M.; Navard, P.; Harabagiu, V.; Pinteala, M.; Simionescu, B. C. Synthesis of Poly(Styrene−dimethylsiloxane) Block Copolymers: Influence of the Phase-Separated Morphologies on the Thermal Behaviors. *Macromolecules* **1998**, *31* (13), 4301–4308. https://doi.org/10.1021/ma971577c.
(95) Gaur, U.; Wunderlich, B. Study of Microphase Separation in Block Copolymers of Styrene and α-Methylstyrene in the Glass Transition Region Using Quantitative Thermal Analysis. *Macromolecules* **1980**, *13* (6), 1618–1625.
(96) Huang, X.; Roth, C. B. Optimizing the Grafting Density of Tethered Chains to Alter the Local Glass Transition Temperature of Polystyrene near Silica Substrates: The Advantage of Mushrooms over Brushes. *ACS Macro Lett.* **2018**, *7* (2), 269–274. https://doi.org/10.1021/acsmacrolett.8b00019.
(97) Grest, G. S. Communication: Polymer Entanglement Dynamics: Role of Attractive Interactions. *J. Chem. Phys.* **2016**, *145* (14), 141101. https://doi.org/10.1063/1.4964617.
(98) Kob, W.; Roldán-Vargas, S.; Berthier, L. Non-Monotonic Temperature Evolution of Dynamic Correlations in Glass-Forming Liquids. *Nature Physics* **2012**, *8* (2), 164–167. https://doi.org/10.1038/nphys2133.
(99) Hocky, G. M.; Berthier, L.; Kob, W.; Reichman, D. R. Crossovers in the Dynamics of Supercooled Liquids Probed by an Amorphous Wall. *Phys. Rev. E* **2014**, *89* (5), 052311. https://doi.org/10.1103/PhysRevE.89.052311.

(100) Pye, J. E.; Roth, C. B. Two Simultaneous Mechanisms Causing Glass Transition Temperature Reductions in High Molecular Weight Freestanding Polymer Films as Measured by Transmission Ellipsometry. *Phys. Rev. Lett.* **2011**, *107* (23), 235701. https://doi.org/10.1103/PhysRevLett.107.235701.
(101) de Gennes, P. G. Glass Transitions in Thin Polymer Films. *Eur. Phys. J. E* **2000**, *2* (3), 201–205. https://doi.org/10.1007/PL00013665.
(102) Cangialosi, D. Dynamics and Thermodynamics of Polymer Glasses. *J. Phys.: Condens. Matter* **2014**, *26* (15), 153101. https://doi.org/10.1088/0953-8984/26/15/153101.
(103) Priestley, R. D.; Cangialosi, D.; Napolitano, S. On the Equivalence between the Thermodynamic and Dynamic Measurements of the Glass Transition in Confined Polymers. *Journal of Non-Crystalline Solids* **2015**, *407*, 288–295. https://doi.org/10.1016/j.jnoncrysol.2014.09.048.
(104) Mangalara, J. H.; Mackura, M. E.; Marvin, M. D.; Simmons, D. S. The Relationship between Dynamic and Pseudo-Thermodynamic Measures of the Glass Transition Temperature in Nanostructured Materials. *The Journal of Chemical Physics* **2017**, *146* (20), 203316. https://doi.org/10.1063/1.4977520.
(105) Tito, N. B.; Lipson, J. E. G.; Milner, S. T. Lattice Model of Mobility at Interfaces: Free Surfaces, Substrates, and Bilayers. *Soft Matter* **2013**, *9* (39), 9403–9413. https://doi.org/10.1039/C3SM51287H.
(106) Phan, A. D.; Schweizer, K. S. Influence of Longer Range Transfer of Vapor Interface Modified Caging Constraints on the Spatially Heterogeneous Dynamics of Glass-Forming Liquids. *Macromolecules* **2019**, *52* (14), 5192–5206. https://doi.org/10.1021/acs.macromol.9b00754.
(107) Kuan, W.-F.; Remy, R.; Mackay, M. E.; Thomas H. Epps, I. I. I. Controlled Ionic Conductivity via Tapered Block Polymer Electrolytes. *RSC Adv.* **2015**, *5* (17), 12597–12604. https://doi.org/10.1039/C4RA15953E.
(108) Soo, P. P.; Huang, B.; Jang, Y.-I.; Chiang, Y.-M.; Sadoway, D. R.; Mayes, A. M. Rubbery Block Copolymer Electrolytes for Solid-State Rechargeable Lithium Batteries. *J. Electrochem. Soc.* **1999**, *146* (1), 32–37. https://doi.org/10.1149/1.1391560.
(109) Sadoway, D. R. Block and Graft Copolymer Electrolytes for High-Performance, Solid-State, Lithium Batteries. *Journal of Power Sources* **2004**, *129*, 1–3. https://doi.org/10.1016/j.jpowsour.2003.11.016.
(110) Weber, R. L.; Ye, Y.; Schmitt, A. L.; Banik, S. M.; Elabd, Y. A.; Mahanthappa, M. K. Effect of Nanoscale Morphology on the Conductivity of Polymerized Ionic Liquid Block Copolymers. *Macromolecules* **2011**, *44* (14), 5727–5735. https://doi.org/10.1021/ma201067h.
(111) Ye, C.; Weiner, C. G.; Tyagi, M.; Uhrig, D.; Orski, S. V.; Soles, C. L.; Vogt, B. D.; Simmons, D. S. Understanding the Decreased Segmental Dynamics of Supported Thin Polymer Films Reported by Incoherent Neutron Scattering. *Macromolecules* **2015**, *48* (3), 801–808. https://doi.org/10.1021/ma501780g.
(112) Pye, J. E.; Rohald, K. A.; Baker, E. A.; Roth, C. B. Physical Aging in Ultrathin Polystyrene Films: Evidence of a Gradient in Dynamics at the Free Surface and Its Connection to the Glass Transition Temperature Reductions. *Macromolecules* **2010**, *43* (19), 8296–8303. https://doi.org/10.1021/ma101412r.
(113) Marvin, M. D.; Lang, R. J.; Simmons, D. S. Nanoconfinement Effects on the Fragility of Glass Formation of a Model Freestanding Polymer Film. *Soft Matter* **2014**, *10* (18), 3166–3170. https://doi.org/10.1039/C3SM53160K.
(114) Forrest, J. A. What Can We Learn about a Dynamical Length Scale in Glasses from Measurements of Surface Mobility? *The Journal of Chemical Physics* **2013**, *139* (8), 084702.
(115) Forrest, J. A.; Dalnoki-Veress, K. When Does a Glass Transition Temperature Not Signify a Glass Transition? *ACS Macro Lett.* **2014**, *3*, 310–314. https://doi.org/10.1021/mz4006217.

(116) Kim, S.; Hewlett, S. A.; Roth, C. B.; Torkelson, J. M. Confinement Effects on Glass Transition Temperature, Transition Breadth, and Expansivity: Comparison of Ellipsometry and Fluorescence Measurements on Polystyrene Films. *Eur. Phys. J. E* **2009**, *30* (1), 83–92. https://doi.org/10.1140/epje/i2009-10510-y.

(117) Mirigian, S.; Schweizer, K. S. Communication: Slow Relaxation, Spatial Mobility Gradients, and Vitrification in Confined Films. *The Journal of Chemical Physics* **2014**, *141* (16), 161103. https://doi.org/10.1063/1.4900507.

(118) Lipson, J. E. G.; Milner, S. T. Percolation Model of Interfacial Effects in Polymeric Glasses. *Eur. Phys. J. B* **2009**, *72* (1), 133–137. https://doi.org/10.1140/epjb/e2009-00324-y.

(119) Rotella, C.; Wübbenhorst, M.; Napolitano, S. Probing Interfacial Mobility Profiles via the Impact of Nanoscopic Confinement on the Strength of the Dynamic Glass Transition. *Soft Matter* **2011**, *7* (11), 5260–5266. https://doi.org/10.1039/C1SM05430A.

(120) Mirigian, S.; Schweizer, K. S. Theory of Activated Glassy Relaxation, Mobility Gradients, Surface Diffusion, and Vitrification in Free Standing Thin Films. *The Journal of Chemical Physics* **2015**, *143* (24), 244705. https://doi.org/10.1063/1.4937953.

(121) Lipson, J. E. G.; Milner, S. T. Local and Average Glass Transitions in Polymer Thin Films. *Macromolecules* **2010**, *43* (23), 9874–9880. https://doi.org/10.1021/ma101099n.